

Nanoscale

Controlled Fractal Growth of Transition Metal Dichalcogenides

Journal:	Nanoscale
Manuscript ID	NR-ART-07-2019-006358.R1
Article Type:	Paper
Date Submitted by the Author:	27-Aug-2019
Complete List of Authors:	Wang, Peijian; University at Buffalo - The State University of New York, physics; Peijian Wang Luo, Siyuan; Shanghai Jiao Tong University, School of Electronic Information and Electrical Engineering Boyle, Lincoln; University at Buffalo - The State University of New York, Physics Zeng, Hao; State University of New York at Buffalo, Department of Physics Huang, Shaoming; Guangdong University of Technology, a. Collaborative Innovation Center of Advanced Energy Materials, School of Materials and Energy

SCHOLARONE™ Manuscripts Page 1 of 14 Nanoscale

Controlled Fractal Growth of Transition Metal Dichalcogenides

Peijian Wang,^{†,‡, ±} Siyuan Luo,^{I,‡, ±} Lincoln Boyle,[‡] Hao Zeng,^{‡*} Shaoming Huang,^{†, *}

†School of Materials and Energy, Guangdong University of Technology, Guangzhou, 510006, P. R. China

‡Department of Physics, University at Buffalo, the State University of New York, Buffalo, NY, 14260, United States

Key Laboratory for Thin Film and Microfabrication of Ministry of Education, School of Electronic Information and Electrical Engineering, Shanghai Jiao Tong University, Shanghai, 200240, China

Abstract

we report controlled fractal growth of atomically thin transition metal dichalcogenides (TMDCs) by chemical vapor deposition, with morphological evolution from dendritic to triangular. Several important growth parameters controlling the fractal dimensions were identified, including the relaxation rate, adhesion coefficient, diffusion anisotropy and growth time. A model based on nucleation, diffusion limited aggregation and relaxation was proposed to explain the morphological evolution. The results of the computational simulation based on this model are in good agreement with the experimental results. Our study sheds light on the growth mechanism of TMDCs and paves the way for growth of TMDCs with improved controllability.

Nanoscale Page 2 of 14

INTRODUCTION

TMDCs, in which transition metal atoms are sandwiched between two layers of chalcogen atoms, possess good carrier mobility, transition from indirect bandgap to direct bandgap upon layer number shrinking, excellent flexibility and transparency. They have attracted significant attention because of their promising prospects for flexible, lightweight and low-power electronics and photonics applications. The planar van der Waals structure bestows the possibility to stack the layers to form heterostructures with greatly enhanced functionalites. Besides, in monolayer TMDCs, the large spin-orbital coupling (SOC) and inversion-symmetry breaking render them two spin-locked valley states in the electronic bands, accessible by circularly polarized light. This valley degree of freedom in TMDCs is appealing for both fundamental physics and applications in information processing. To the planar van der Waals structure bestows the possibility to stack the layers to form heterostructures with greatly enhanced functionalites.

Various proposed applications of TMDCs require good attainability of atomically thin layers with controlled thickness and morphology. For example, for many device applications, uniform, large area single crystal monolayers are needed. On the other hand, fractal TMDCs with large number of exposed edge sites can be highly active for catalytic applications. ¹⁵ Synthesis with accurate control of morphology thus becomes a key research direction in the area of TMDCs. Due to its simplicity, scalability and low cost, chemical vapor deposition (CVD) is one of the most commonly used approaches for the growth of atomically thin TMDCs. 16 Extensive efforts have been devoted to the CVD growth and shape evolution of TMDCs. For example, Liu et al. studied the effect of varying temperature and growth duration on the flake shape, suggesting that higher temperatures change the shape from triangles into hexagons.¹⁷ Wang et al. used four Si substrates in a queue in CVD to study the shape evolution of monolayer MoS₂ crystals. They found transformation of shape from triangles to hexagons then back to triangles along the gas flow direction, which they attribute to deficiency of Mo or S that lead to different growth rate of Mo and S terminations. ¹⁸ Cain et al. utilized high-resolution scanning transmission electron microscopy (STEM) and X-ray energy dispersive spectroscopy (EDS) mapping to reveal that the nuclei in CVD growth are oxi-chalcogenide/TMDC core-shell nanoparticles. 19 Understanding growth mechanisms is the key for improving controllability and quality of CVD grown TMDCs.¹ For example, Rajan et al. applied the Kinetic Monte Carlo (KMC) method with a terrace-ledgekink model, assuming the surface to be a terrace with unsaturated bonds. 18, 20 Nie et al. used KMC to study the morphology with respect to temperature, and chalcogen/metal stoichiometry.²¹ However, the evolution of morphologies, and factors governing the morphologies such as monomer adhesion, cooling rate and diffusion anisotropy remain to be fully elucidated and tightly connected to experiments. In particular, most previous publications focus on regularshaped TMDCs such as triangles and hexagons, while there are scarce reports of fractal growth.

In this work, we use WS_2 as an example to systematically study the controlling factors governing the morphological evolution from dendrites to triangles during the growth of atomically thin TMDCs. Based on observations of changes in morphologies as a function of growth parameters including cooling rate, growth time, we propose a physical picture of the growth involving nucleation, diffusion limited aggregation (DLA) and relaxation. Computational simulation based on the model reproduces experimental results. We further verify the model by growing large area triangles by judicious control of the relaxation process. The ability to produce TMDC atomic

Page 3 of 14 Nanoscale

layers with controlled fractal dimension can enable further applications of the fractal TMDCs materials, such as catalysis and sensing.

RESULTS AND DISCUSSION

Experimental results

We carried out CVD growth in the set-up illustrated in Figure S1. We employed CS₂ carried by argon gas as the sulfur source, instead of the S powder in conventional CVD synthesis. The temperature profile was set as follows: it was first increased to the growth temperature of 920 °C at a ramping rate of 27°C/min; the temperature was kept at 920 °C for 10 min. After the 10 min

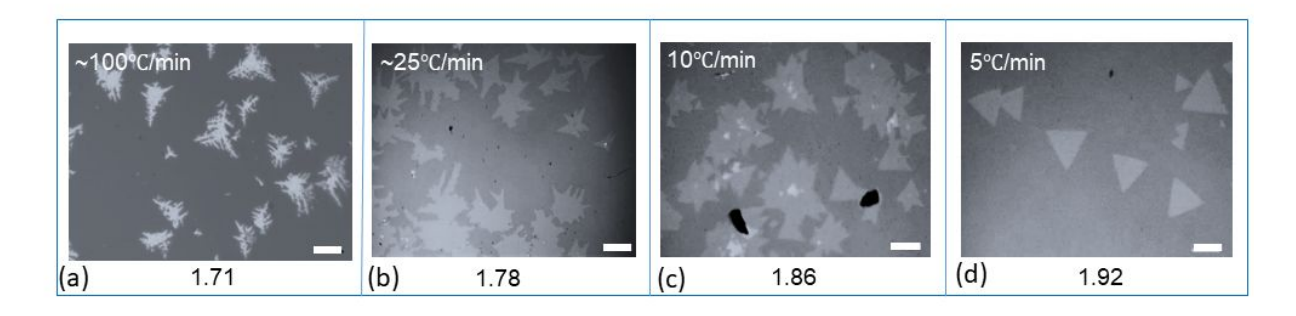


Figure 1. The optical microscope images of atomically thin WS_2 grown at different cooling rate with otherwise identical conditions (labeled on the top-left of each figure). The cooling rate of 100° C/min (a) was obtained by opening the lid of the furnace immediately after finishing heating. The cooling rate of 25° C/min (b) was by cooling down naturally with the lid closed. The cooling rate of 10° C/min (c) and 5° C/min (d) was set by the temperature controller. The fractal dimensions are labeled underneath the images. All scale bars are 50° µm. All other experimental conditions are described explicitly in the

growth, the furnace was cooled down at various cooling rates from 5 to 100 °C/min. A sapphire substrate was placed upside down on a graphite boat, which contains the WO₃ powder. Note the utilization of CS₂ as S source for the growth of atomically thin TMDCs flakes has not been reported, as far as we know. Replacing S by CS2 makes it easier to control the sulfurization process, by switching on and off the S source on demand. One can control the supply of the S source precisely as the desired growth temperature is reached, so that the crystallinity of the TMDCs can be controlled. It is also more accurate to control the S partial pressure by controlling the flow rate of the gas carrying the CS₂; while in conventional synthesis, the S partial pressure is controlled by S evaporation temperature and small variations in temperature can lead to large fluctuations in S concentration. It is found that cooling rate strongly influences the morphology of the grown atomically thin TMDCs. Figure 1 are the optical microscope images showing morphological evolution of the TMDCs grown at different cooling rate. The fastest cooling rate in Figure 1a is 100 °C/min in the temperature range of 900 °C-600 °C, obtained by opening the lid of the furnace immediately after heating. With this process, the as-grown morphology of the sample is frozen. As seen in Figure 1a, highly dendritic features, involving branches with selfsimilarity, are observed. For a slow cooling rate of 5°C/min, on the other hand, the morphology

Nanoscale Page 4 of 14

turns into regular triangles, with sharp edges (Figure 1(d)). For intermediate cooling rates, the morphologies are somewhere in between the dendrites and triangles. To quantify the morphological evolution, we calculated the fractal dimensions D using the box counting method. Briefly, using different sized boxes to cover the feature, D is defined as $D = \lim_{\log(\varepsilon) \to 0} \frac{\log N(\varepsilon)}{\log(\varepsilon)}$, where

 ε is the side length of the boxes and N(ε) is the number of boxes required to cover the feature. Fractal dimension is a quantitative measure of the space filling capability of a pattern, which is 1 for a straight line and 2 for a square (Figure S2). D is found to be 1.71 for the sample in Figure 1a, and increases monotonically with decreasing cooling rate. D is found to be 1.92 for the cooling rate of 5 °C/min, which is close to two-dimensional. This can be understood as follows: the triangular shape is the most thermodynamically stable morphology of atomically thin TMDCs, determined by the directionality of chemical bonding and interactions of the orbitals of the hexagonal lattice. During a CVD growth processes, the availability of W and S precursors is hardly stoichiometric. Because of faster growth rate of either W-terminated zigzag edge or S-terminated zigzag edge due to deficiency of one of the elements, the most frequently observed thermodynamically stable shape is triangular instead of hexagonal. Previous work has shown that at the growth temperature of 600 to 700 °C, the atoms can diffuse by large distances up to many microns in the growth of MoS₂. A slower cooling rate would allow the atoms to diffuse more freely to find their equilibrium position. Thus, it will favor formation of thermodynamically equilibrium shape.

To investigate the morphological evolution at different stages of growth, optical microscope images were taken for samples with different growth time. The cooling rate were kept at

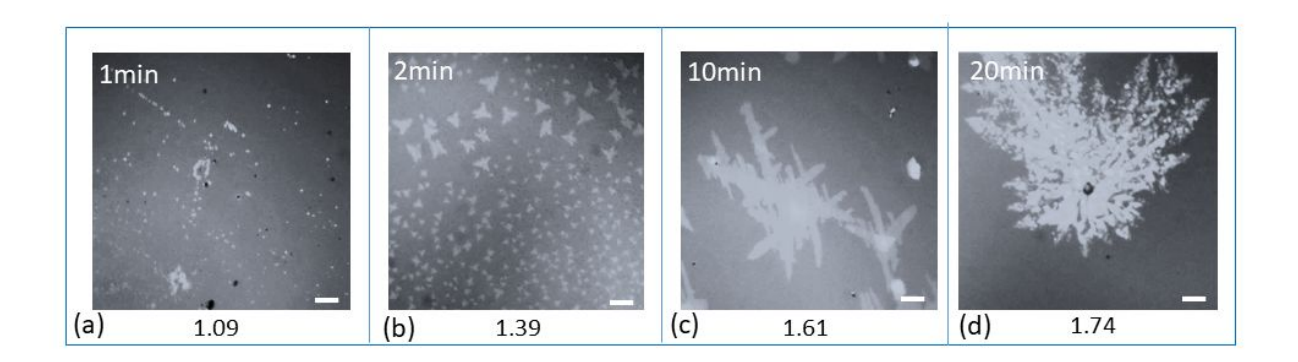


Figure 2. Optical microscope images showing morphological evolution as a function of growth time. The duration is labeled in the top-left corner. The fractal dimensions are labeled at the bottom. Scalebars are all $10\mu m$.

100 °C/min. Figure 2 shows the morphological evolution at different growth stages. It can be seen that with increasing growth time, the size of the fractal features increased and the fractal dimension monotonically increased. Raman and photoluminescence (PL) spectral characteristics in Figures S3 and S4, SI show that the features in the early stage (Figure 2a, 2b) are monolayer WS₂. The fractal dimension D is found to be 1.09 for the growth time of 1 min (Figure 2a), and increases with increasing growth time. D is found to increase to 1.74 for the growth time of 20 mins, as shown in Figure 2d.

Page 5 of 14 Nanoscale

Physical picture of the growth dynamics

Based on the empirical observations described above, we propose a physical picture of the growth dynamics, shown schematically in Figure 3a: First, nucleation sites are formed randomly on the substrate. Second, the growth of nuclei undergoes a diffusion limited aggregation (DLA) process: ²⁵ With a monomer serving as the nucleation center, another monomer is launched and diffuses on the surface, which can be described by random walk; after the incoming monomer colliding with an existing structure, it adheres to become part of the aggregate. Continued diffusion and adhesion forms dendritic/fractal structure. On the other hand, the most thermodynamically stable morphology of monolayer TMDCs is triangular. The morphological evolution from fractals to triangles suggests that there is a competition between the DLA growth

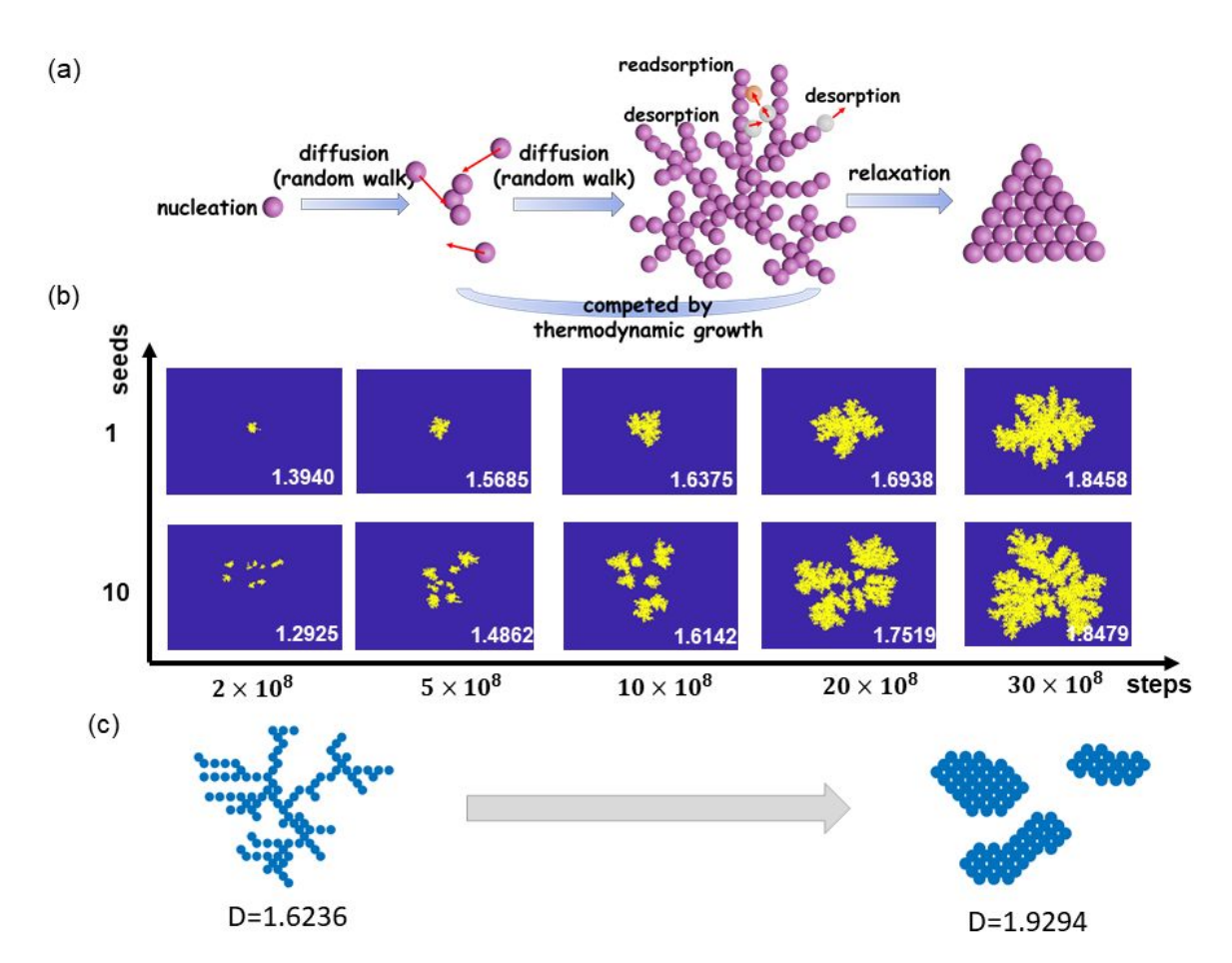


Figure 3. (a) The schematic displays the physical picture of the CVD growth process: nucleation, diffusion limited aggregation which competes with thermodynamic growth; (b) The simulation results using the DLA algorithm, displaying evolution with different seed numbers (1, 10) and step numbers $(2 \text{ to } 30 \times 10^8)$. The number at the lower-right corner in each frame indicates the fractal dimension of the dendritic structure in the frame. (c) The shape evolution from a fractal to a more regular shape after the following algorithm is executed for 1000 times: the fractal with 100 pixels was formed in the hexagonal lattice by the DLA algorithm, the monomers with 1 or 2 nearest neighbor numbers (NNN) then desorb from the existing structure, diffuse and readsorb to sites with larger NNN.

Nanoscale Page 6 of 14

and the thermodynamic growth.²³ Finally, during the slow cooling process upon which the supply of precursors was cut off, the as-grown dendritic structure undergoes a relaxation process, in which the shape morphs into the most thermodynamically stable triangles.

To confirm the proposed physical picture, we carried out computational simulations, based on the DLA algorithm. For the algorithm, ²⁶ we set up a stochastic routine to simulate the growth dynamics in Matlab: first, a nucleation center was set at the origin of the coordinate, then a random walker was launched (WS₂ monomer) at a random position and allowed to diffuse randomly until it is in contact with the previously formed structure.²⁵ It then adhered to the existing structure with a preset probability, parameterized as the adhesion coefficient. Once it got stuck, another walker was launched and proceeded until it encountered the existing structure (for details, see Methods). Note that at the growth temperature, the length scale of the diffusion on the substrate is much larger than the atomic bonding spacing, and the diffusion can be regarded as from any direction. For simplicity, we had not taken into account the crystal symmetry, and instead focused on the growth kinetics. To study the morphological evolution, we simulated the growth with different number of random walk steps, representing different growth time as they are proportional to each other. Figure 3a is a schematic of the growth process. Initially, the nucleation sites are created by adsorption of small number of monomers. Second, the monomers diffuse on the surface of the substrates and are assembled by the diffusion limited aggregation, which competes with the thermodynamic growth that favors more regular shape. The fractal dimension increases and gets closer to that of a 2D planar object. This is because the monomers that go deep into the dendrites have increased probability to stick after multiple collisions. While those at the outer boundaries have more tendency to desorb since the direction of diffusion is random, which decreases the chance of second collision. Finally, after the cease of the supply of the precursor and as the temperature is lowered, the as-grown structure undergoes a relaxation process, in which it evolves into the thermodynamically more stable shape. Figure 3b shows the simulation results with different seed numbers (1 and 10) and step numbers (2 to 30×10^8), in which the relaxation was not considered. As can be seen from Figure 3b, with increasing step number, the size of the structure clearly increases. In Fig. 3c, the simulation of the relaxation process was also conducted. The originally stuck monomers with fewer nearest neighbor numbers (1 or 2, vertex sites or edge sites) in the fractal were allowed to desorb, diffuse and then readsorb. As a result, they tend to adhere to sites with larger nearest neighbor numbers in the hexagonal lattice. This larger bonding number lowers the system energy. Fig. 3c shows clearly that after the relaxation, the morphology evolves to be more regular and compact, with increased fractal dimension from 1.62 to 1.93.

Page 7 of 14 Nanoscale

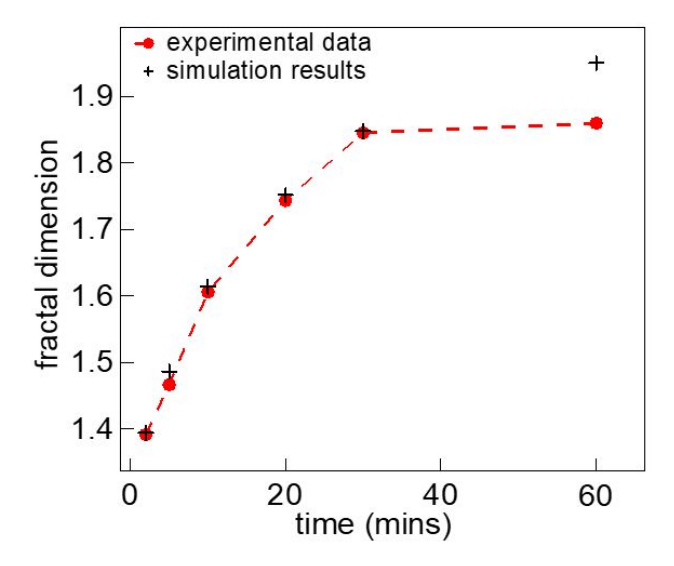


Figure 4. The time dependence of the fractal dimension, comparing the experimental data with the simulation results in the case of seed number =10 in Figure 3b. Simulation result for 1 hour's growth is shown in Figure S6.

Figure 4 shows the fractal dimension as a function of growth time, where the experimental data are shown as red dots and simulation results are black crosses (the seed number is 10). It can be seen that the experimental data are in good agreement with the simulation results. In the simulation, the fractal dimension approaches 2 at long time. However, the experimental data show a leveling-off to ~ 1.86 . The deviation of experimental data from simulation results at t = 60min is likely due to the tendency of 3D growth in experiments, which was not considered in the simulation in Fig. 4. In a real growth process, the excess monomers can stick to the top of the layer, rather than sticking only in the two-dimensional plane. Thus, continued supply of precursor will usually lead to overgrowth. In order to achieve large area monolayer growth with uniform shape and higher fractal dimension, judicious control of the relaxation process may be needed; this will be discussed towards the end of the paper. Moreover, Figure S5a shows the simulation results with different seed numbers (1, 5, 50) and adhesion coefficients (1, 0.1, 0.01, 0.001, 0.0001), the parameter of probability of sticking of monomers in a collision event. As seen from figure S5a, with high adhesion coefficients, the morphology shows strong dendritic features with smaller fractal dimensions. When the adhesion coefficient decreases, the aggregates become more and more compact, and the fractal dimension increases. In Figure S7, in the simulation conducted in the hexagonal lattice, it clearly shows the same trend that as the adhesion coefficient decreases, the fractal dimension increases. It can be rationalized as following: as the adhesion coefficient decreases, the number of collisions it takes for a monomer to stick increases. As the collision is isotropic in all directions, the shape becomes more isotropic and compact.

The gas-flow induced diffusion anisotropy was considered in the simulation as well. A higher probability of 0.3 walking to the right was assigned to the DLA simulation, representing the gas flow direction. A lower probability 0.2 to the left was set as against the gas flow direction. The

Nanoscale Page 8 of 14

results (Figure S5b) show anisotropy in the growth, with bloom-like dendrites. Indeed, the bloom-like dendrites were found experimentally, when the flow rate of the carrier gas was increased to 60 sccm from 20 sccm (Figure S5c).

These simulation results indicate important controlling factors governing the morphology of CVD grown monolayer TMDCs: adhesion coefficients, diffusion anisotropy, seed number and growth duration. To obtain dendritic shape, preferred for catalytic applications, substrates with higher adhesion coefficient or that with pre-deposited seeds should be used. To grow more compact shape instead, substrates with lower adhesion coefficient and smooth surface free of debris should be used. Moreover, larger size and higher fractal dimension are induced by longer growth duration.

Raman spectroscopy as a quantitative measure of fractal dimensions

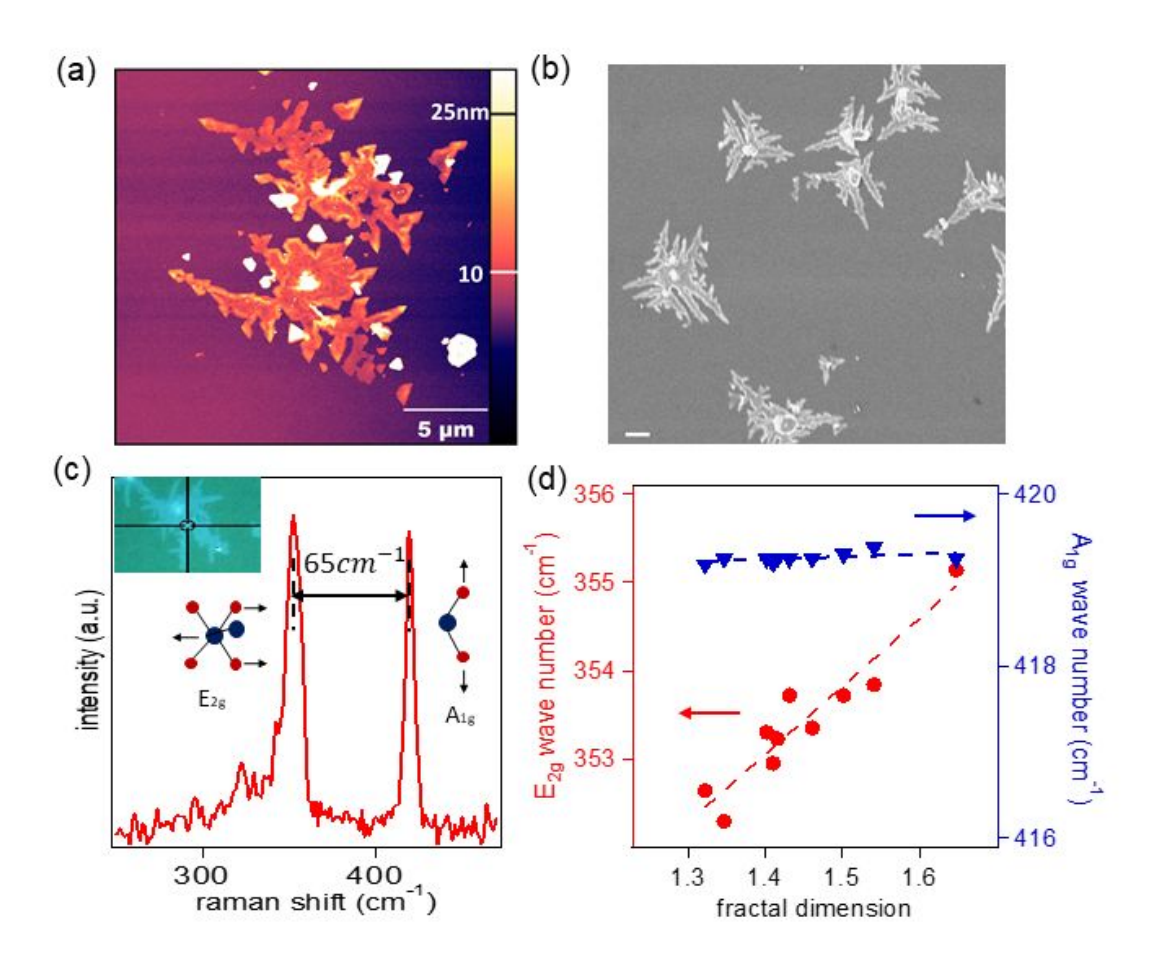


Figure 5. (a) An AFM image of WS_2 showing dendritic features. The scale bar is 5 μ m. (b) An SEM image of WS_2 with dendritic features. The scale bar is 2 μ m. (c) A Raman spectrum of a fractal monolayer. Inset shows the position where the Raman spectrum was measured. (d) Correlation of E_{2g} peak position (left axis for the red circles) and A_{1g} peak position (right axis for the blue triangles) with the fractal dimension (the Raman spectra are in Figure S9).

U

Page 9 of 14 Nanoscale

We employed atomic force microscopy (AFM), scanning electron microscopy (SEM) and Raman spectroscopy to further characterize the fractal features of monolayer WS₂. The AFM morphological image (Figure 5a) and the scanning electron microscope (SEM) images (Figure 5b) show branched, self-similar characteristics of the dendritic feature and also the fractal edges. Figure 5c shows a typical Raman spectrum of a monolayer WS₂ with fractal features. It is found that the A_{1g} and E_{2g} modes appear at 354 and 419 cm⁻¹, with a wavenumber difference of 65 cm⁻¹, revealing its monolayer thickness.²⁷⁻²⁸

Figure S8, SI shows the Raman intensity map of a dendrite at two peaks: 354, 419 cm^{-1} , suggesting relative uniformity. The peak positions of the E_{2g} and A_{1g} , are plotted as a function of fractal dimension in Figure 5d. The frequency of the E_{2g} peak increases approximately linearly with increasing fractal dimension. On the other hand, the A_{1g} peak positions are nearly dimension independent. This interesting observation can be understood as follows: comparing to monolayer triangles, the dendritic features on average will have fewer nearest neighbor atoms. This should lead to softening of the in-pane E_{2g} vibration mode. The lower the fractal dimension, the higher the missing nearest neighbor number, and thus the larger the shift towards lower frequencies. On the other hand, the out-of-plane A_{1g} mode should be less affected by the nearest neighbor numbers. Therefore, the position of the E_{2g} peak can be used as a quantitative measure of the fractal dimension of TMDCs monolayers.

Growth of large area TMDCs by controlling the relaxation process

Large area monolayer TMDCs allows parallel fabrication of devices by photolithography, and therefore are highly desirable. While large area samples can be obtained by longer growth time,

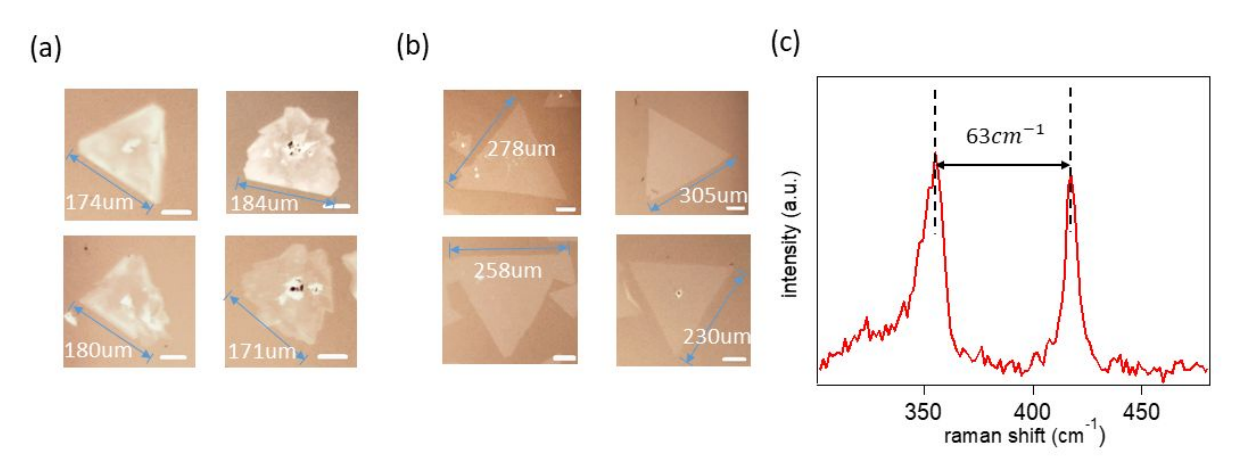


Figure 6. (a) The optical microscopic images of typical flakes with a total growth time of 25 mins; (b) The optical microscopic images of typical flakes of growth incorporating a relaxation process. The CS₂ flow was cut off after 10 mins' growth. After the furnace was cooled down naturally to 500°C, it was heated up again to the growth temperature. The CS₂ flow was turned back on for an additional growth of 15 mins. (c) The Raman spectrum taken on a single flake in (b). The scale bars are all 50μm.

significant overgrowth may occur. Figure 6a shows the result of WS₂ with a total growth time of

Nanoscale Page 10 of 14

25 mins with constant flow of CS₂ (detailed conditions are described in the Methods). With prolonged growth time, it can be seen that significant overgrowth occurred. Based on the physical model we proposed, we design an experiment to address the overgrowth problem and obtain large area monolayers of WS2. In this approach, we inserted an intermediate relaxation step in between two consecutive growth steps. The procedure is as follows: After 10 min of growth at 920 °C, the CS2 flow was cut off. The temperature was naturally cooled down to 500 °C. As explained above, slow cooling can help the monomers to diffuse to its most thermodynamically stable sites, and favors the growth of regular shaped monolayer TMDCs. The temperature was then raised to the growth temperature of 920 °C, at which time the CS₂ flow was turned back on. The growth continues for another 15 mins, after which the sample was cooled at a rate of 5 °C/min for 10 mins. Finally, the furnace was cooled down naturally to the room temperature. Figure 6b shows the morphology of the samples grown by the new procedure. While in the one step growth, the typical flake size was around 170-180 µm (Figure 6a); the flake size of the sample grown by inserting a relaxation step was noticeably larger, reaching 200-300 µm (Figure 6b). More importantly, the surface of the flakes is cleaner, with significantly less multilayer overgrowth. The Raman spectrum as shown in Fig. 6c revealed that the flakes are monolayer WS₂. These results validate the physical picture we proposed.

CONCLUSION

In conclusion, we conducted experimental and computational investigations on the controlled fractal growth of monolayer WS_2 . CS_2 was used as the S source in the growth to yield better controllability. By observing growth morphology under different relaxation rates and growth time, we propose a physical picture of the growth mechanism: it undergoes three stages, namely nucleation, diffusion limited aggregation and relaxation. Computer simulation based on DLA algorithm confirmed the proposed model, and further pointed out additional factors affecting the morphology including seed number, adhesion coefficients and diffusion anisotropy. The E_{2g} mode of the Raman spectrum was used to quantify the fractal dimension. On the basis of the physical model, we judiciously controlled the relaxation process, and achieved large-scale flakes beneficial for device applications.

Page 11 of 14 Nanoscale

METHODS

CVD synthesis of WS₂:

The sapphire substrates were cleaned in acetone for 10mins and then rinsed by ethanol, followed by air blow drying. In a typical growth, 3mg WO₃ powder was loaded into a graphite boat. The substrate was supported on the graphite boat, facing downward. The boat and the substrate were placed in the center of the quartz tube. The temperature profile was programmed as follows: initially the quartz tube was flushed with the argon gas by 10 minutes, at the temperature of 100°C. The quartz tube was then heated to 920°C, with a ramping rate of 27°C/min. Next, the CS₂ carried by argon gas was introduced at a flow rate of 20 sccm. The reaction took place at 920°C for 10 mins. At the end of the growth, the CS₂ was turned off and system was flushed by argon gas again. The cooling rate ranged from 5 to 100 °C/min. The fastest cooling rate were achieved by opening the lid immediately following the growth.

DLA algorithm details:

Simulation method in Figure 3b, Figure 4 and Figure S5: Initially, a lattice of 500×500 was set. Next, for the seed number of 1, one nucleation center was settled at the center of the frame; while for the seed number of 10, ten seeds were settled randomly in the box of 100×100 at the center of the frame. A random walker monomer was then launched from a random unoccupied position. Afterwards, it started random walk in four directions: up, down, left and right, with equal probability of 0.25. If this monomer moved out of the frame boundary, a new "walker" was launched. If the walker got in contact with the existing structure, it adhered to the existing structure by a pre-defined probability as adhesion coefficient; otherwise, the monomer kept moving. The aforementioned procedure was repeated until the number of steps reached the preset value. For the simulation of anisotropic diffusion, the probability of moving along the gas flow direction was set as 0.3; meanwhile, the probability going in the opposite direction of the gas flow was set as 0.2. The probabilities of going up and down were both 0.25.

AUTHOR INFORMATION

Corresponding Author:

*Hao Zeng, email: haozeng@buffalo.edu

*Shaoming Huang, email: smhuang@gdut.edu.cn

Author contributions:

[⊥]P.W. and S.L. authors contribute equally to this paper.

ACKNOWLEDGEMENTS

We acknowledge support from Nature Science Foundation of China (NSFC 51420105002 and 51672193) and US National Science Foundation DMR-1104994 and CBET-1510121.

Nanoscale Page 12 of 14

REFERENCES

- 1. Li, H.; Li, Y.; Aljarb, A.; Shi, Y.; Li, L. J., Epitaxial Growth of Two-Dimensional Layered Transition-Metal Dichalcogenides: Growth Mechanism, Controllability, and Scalability. *Chem Rev* **2018**, *118* (13), 6134-6150.
- 2. Huo, N.; Kang, J.; Wei, Z.; Li, S.-S.; Li, J.; Wei, S.-H., Novel and Enhanced Optoelectronic Performances of Multilayer MoS₂-WS₂ Heterostructure Transistors. *Advanced Functional Materials* **2014**, *24* (44), 7025-7031.
- 3. Yoon, Y.; Ganapathi, K.; Salahuddin, S., How Good Can Monolayer MoS₂ Transistors Be? *Nano Lett* **2011**, *11* (9), 3768-73.
- 4. Wang, Q. H.; Kalantar-Zadeh, K.; Kis, A.; Coleman, J. N.; Strano, M. S., Electronics and Optoelectronics of Two-Dimensional Transition Metal Dichalcogenides. *Nat Nanotechnol* **2012**, *7* (11), 699-712.
- 5. Huang, H.; Xu, W.; Chen, T.; Chang, R. J.; Sheng, Y.; Zhang, Q.; Hou, L.; Warner, J. H., High-Performance Two-Dimensional Schottky Diodes Utilizing Chemical Vapour Deposition-Grown Graphene-MoS₂ Heterojunctions. *ACS Appl Mater Interfaces* **2018**, *10* (43), 37258-37266.
- 6. Wang, L.; Meric, I.; Huang, P. Y.; Gao, Q.; Gao, Y.; Tran, H.; Taniguchi, T.; Watanabe, K.; Campos, L. M.; Dean, C. R.; et.al.;, One-Dimensional Electrical Contact to a Two-Dimensional Material. *Science* **2013**, *342*, 614-617.
- 7. Yang, T.; Zheng, B.; Wang, Z.; Xu, T.; Pan, C.; Zou, J.; Zhang, X.; Qi, Z.; Liu, H.; Feng, Y.; Hu, W.; Miao, F.; Sun, L.; Duan, X.; Pan, A., Van der Waals Epitaxial growth and Optoelectronics of Large-scale WSe₂/SnS₂ Vertical Bilayer p-n Junctions. *Nat Commun* **2017**, *8* (1), 1906.
- 8. Wang, G.; Li, L.; Fan, W.; Wang, R.; Zhou, S.; Lü, J.-T.; Gan, L.; Zhai, T., Interlayer Coupling Induced Infrared Response in WS2/MoS2 Heterostructures Enhanced by Surface Plasmon Resonance. *Advanced Functional Materials* **2018**, *28* (22), 1800339.
- 9. Gibney, E., 2D or not 2D. *Nature* **2015**, *522*, 274-276.
- 10. Mak, K. F.; He, K.; Shan, J.; Heinz, T. F., Control of Valley Polarization in Monolayer MoS₂ by Optical Helicity. *Nat Nanotechnol* **2012**, *7* (8), 494-8.
- 11. Xiao, D.; Liu, G. B.; Feng, W.; Xu, X.; Yao, W., Coupled Spin and Valley Physics in Monolayers of MoS₂ and Other Group-VI Dichalcogenides. *Phys Rev Lett* **2012**, *108* (19), 196802.
- 12. Wu, Y. J.; Shen, C.; Tan, Q. H.; Shi, J.; Liu, X. F.; Wu, Z. H.; Zhang, J.; Tan, P. H.; Zheng, H. Z., Valley Zeeman Splitting of Monolayer MoS₂ Probed by Low-Field Magnetic Circular Dichroism Spectroscopy at Room Temperature. *Applied Physics Letters* **2018**, *112* (15), 153105.
- 13. Zhao, C.; Norden, T.; Zhang, P.; Zhao, P.; Cheng, Y.; Sun, F.; Parry, J. P.; Taheri, P.; Wang, J.; Yang, Y.; Scrace, T.; Kang, K.; Yang, S.; Miao, G. X.; Sabirianov, R.; Kioseoglou, G.; Huang, W.; Petrou, A.; Zeng, H., Enhanced Valley Splitting in Monolayer WSe₂ due to Magnetic Exchange Field. *Nat Nanotechnol* **2017**, *12* (8), 757-762.
- 14. Urbaszek, B.; Marie, X., Divide and Polarize. *Nature Physics* **2015**, *11* (2), 94-95.
- 15. Zhang, Y.; Liu, K.; Wang, F.; Shifa, T. A.; Wen, Y.; Wang, F.; Xu, K.; Wang, Z.; Jiang, C.; He, J., Dendritic Growth of Monolayer Ternary WS₂(1-x)Se₂x Flakes for Enhanced Hydrogen Evolution Reaction. *Nanoscale* **2017**, *9* (17), 5641-5647.
- 16. Zhang, X.; Xiao, S.; Nan, H.; Mo, H.; Wan, X.; Gu, X.; Ostrikov, K. K., Controllable one-step growth of bilayer MoS₂-WS₂/WS₂ Heterostructures by Chemical Vapor Deposition. *Nanotechnology* **2018**, *29* (45), 455707.
- 17. Liu, B.; Fathi, M.; Chen, L.; Abbas, A.; Ma, Y.; Zhou, C., Chemical Vapor Deposition Growth of Monolayer WSe₂ with Tunable Device Characteristics and Growth Mechanism Study. *ACS Nano* **2015**, *9*, 6119-6127.

Page 13 of 14 Nanoscale

- 18. Wang, S.; Rong, Y.; Fan, Y.; Pacios, M.; Bhaskaran, H.; He, K.; Warner, J. H., Shape Evolution of Monolayer MoS₂ Crystals Grown by Chemical Vapor Deposition. *Chemistry of Materials* **2014**, *26* (22), 6371-6379.
- 19. Cain, J. D.; Shi, F.; Wu, J.; Dravid, V. P., Growth Mechanism of Transition Metal Dichalcogenide Monolayers: The Role of Self-Seeding Fullerene Nuclei. *ACS Nano* **2016**, *10* (5), 5440-5.
- 20. Govind, A. G.; Warner, J. H.; Blankschtein, D.; Strano, M. S., Generalized Mechanistic Model for the Chemical Vapor Deposition of 2D Transition Metal Dichalcogenide Monolayers. *ACS Nano* **2016**, *10* (4), 4330-44.
- 21. Nie, Y.; Liang, C.; Zhang, K.; Zhao, R.; Eichfeld, S. M.; Cha, P.-R.; Colombo, L.; Robinson, J. A.; Wallace, R. M.; Cho, K., First Principles kinetic Monte Carlo Study on the Growth Patterns of WSe₂ Monolayer. *2D Materials* **2016**, *3* (2), 025029.
- 22. Maugeri, L.; DiNuzzo, M.; Moraschi, M.; Nicaise, C.; Bukreeva, I.; Mangini, F.; Giove, F.; Cedola, A.; Fratini, M., Fractal Dimension Analysis of High-Resolution X-Ray Phase Contrast Micro-Tomography Images at Different Threshold Levels in a Mouse Spinal Cord. *Condensed Matter* **2018**, *3* (4), 48.
- 23. Chen, Z.; Wang, L.-W., Material Genome Explorations and New Phases of Two-Dimensional MoS₂, WS₂, and ReS₂ Monolayers. *Chemistry of Materials* **2018**, *30* (18), 6242-6248.
- 24. Taheri, P.; Wang, J.; Xing, H.; Destino, J. F.; Arik, M. M.; Zhao, C.; Kang, K.; Blizzard, B.; Zhang, L.; Zeng, H.; et.al.;, Growth mechanism of largescale MoS₂ Monolayer by Sulfurization of MoO₃ Film. *Materials Research Express* **2016**, *3* (7), 075009.
- 25. Witten, T. A.; Sander, L. M., Diffusion-Limited Aggregation, a Kinetic Critical Phenomenon. *Physical Review Letters* **1981**, *47* (19), 1400-1403.
- 26. Sander, L., Advanced Condensed Matter Physics. Cambridge University Press: New York, 2009.
- 27. Zeng, H.; Liu, G. B.; Dai, J.; Yan, Y.; Zhu, B.; He, R.; Xie, L.; Xu, S.; Chen, X.; Cui, X.; et.al.;, Optical Signature of Symmetry Variations and Spin-Valley Coupling in Atomically Thin Tungsten Dichalcogenides. *Scientific Reports* **2013**, *3*, 1-5.
- 28. Withers, F.; Bointon, T. H.; Huadson, D. C.; Craciun, M. F.; Russo, S., Electron Transport of WS₂ Transistors in a Hexagonal Boron Nitride Dielectric Environment. *Scientific Reports* **2014**, *4*, 1-5.

Nanoscale Page 14 of 14

Table of Contents figure:

